

## Phase transition-like behavior of magnetospheric substorms: Global MHD simulation results

X. Shao,<sup>1</sup> M. I. Sitnov,<sup>1</sup> S. A. Sharma,<sup>1</sup> K. Papadopoulos,<sup>1</sup> C. C. Goodrich,<sup>1</sup> P. N. Guzdar,<sup>2</sup>  
G. M. Milikh,<sup>1</sup> M. J. Wiltberger,<sup>3</sup> and J. G. Lyon<sup>3</sup>

Received 27 December 2001; revised 24 June 2002; accepted 21 October 2002; published 25 January 2003.

[1] Using nonlinear dynamical techniques, we statistically investigate whether the simulated substorms from global magnetohydrodynamic (MHD) models have a combination of global and multiscale features, revealed in substorm dynamics by *Sitnov et al.* [2000] and featured the phase transition-like behavior. We simulate seven intervals of total duration of 280 hours from the data set used in the above works [*Bargatze et al.*, 1985]. We analyze the input–output ( $\nu B_s$ –pseudo AL index) system obtained from the global MHD model and compare the results to those inferred from the original set ( $\nu B_s$ –observed AL index). The analysis of the coupled  $\nu B_s$ –pseudo AL index system shows the first-order phase transition map, which is consistent with the map obtained for the  $\nu B_s$ –observed AL index system. Although the comparison between observations and global MHD simulations for individual events may vary, the overall global transition pattern during the substorm cycle revealed by singular spectrum analysis (SSA) is statistically consistent between simulations and observations. The coupled  $\nu B_s$ –pseudo AL index system also shows multiscale behavior (scale-invariant power law dependence) in SSA power spectrum. Besides, we find the critical exponent of the nonequilibrium transitions in the magnetosphere, which reflects the multiscale aspect of the substorm activity, different from power law frequency of autonomous systems. The exponent relates input and output parameters of the magnetosphere. We also discuss the limitations of the global MHD model in reproducing the multiscale behavior when compared to the real system. **INDEX TERMS:** 2753 Magnetospheric Physics: Numerical modeling; 2447 Ionosphere: Modeling and forecasting; 2788 Magnetospheric Physics: Storms and substorms; 3220 Mathematical Geophysics: Nonlinear dynamics; 2736 Magnetospheric Physics: Magnetosphere/ionosphere interactions; **KEYWORDS:** magnetospheric substorm, global MHD simulation, nonlinear dynamics, phase transition-like behavior

**Citation:** Shao, X., M. I. Sitnov, S. A. Sharma, K. Papadopoulos, C. C. Goodrich, P. N. Guzdar, G. M. Milikh, M. J. Wiltberger, and J. G. Lyon, Phase transition-like behavior of magnetospheric substorms: Global MHD simulation results, *J. Geophys. Res.*, 108(A1), 1037, doi:10.1029/2001JA009237, 2003.

### 1. Introduction

[2] The global behavior of the magnetosphere in response to the solar wind input is known to be coherent to a large extent [*Sharma*, 1995; *Klimas et al.*, 1996]. The largest substorm phenomena, e.g., global reconfiguration, are in reasonable agreement with low-dimensional magnetospheric models and in particular those of inverse bifurcations. Models of the magnetospheric behavior during substorms, e.g., near-Earth neutral line (NENL) model [*Baker et al.*, 1996], imply its global coherence and self-organization.

[3] At the same time there is growing evidence of hierarchical multiscale aspect of magnetospheric activity represented first of all in the form of various power law spectra [*Tsurutani et al.*, 1990; *Takalo et al.*, 1993; *Ohtani et al.*, 1995, 1998; *Lui*, 1998; *Uritsky et al.*, 2001]. This evidence has led to models [*Consolini*, 1997; *Chapman et al.*, 1998; *Lui et al.*, 2000; *Klimas et al.*, 2000] based on the hypothesis that the magnetosphere is in a state of self-organized criticality (SOC) [*Bak et al.*, 1987]. The original SOC model is based on the model of sandpiles, where the critical state is characterized by power law fluctuation spectra. Briefly, a system is in a state of SOC when the statistics of the energy release events (avalanches) reveal no characteristic length or timescale and, as a result, the appropriate spectra obey power laws. *Sergeev et al.* [1996] give a detailed review on the multiscale aspects of the substorm activity.

[4] Both the self-organization and the SOC models have their limitations. The self-organization model cannot explain the multiscale behavior of the substorms. The typical SOC model is essentially independent of the driver

<sup>1</sup>Department of Astronomy, University of Maryland, College Park, Maryland, USA.

<sup>2</sup>Institute for Plasma Research, University of Maryland, College Park, Maryland, USA.

<sup>3</sup>Department of Physics, Dartmouth College, Hanover, New Hampshire, USA.

and thus is autonomous, which is not the case with the Earth's magnetosphere. The SOC models are too simplified to capture the global coherent behavior of the magnetosphere. It has been found recently that the global coherent (self-organization) and multiscale (SOC) aspects of the magnetospheric behavior can be reconciled in terms of nonequilibrium phase transition [Sitnov *et al.*, 2000, 2001], consistent with earlier phenomenological models of substorm activity [Sergeev *et al.*, 1996] and magnetospheric convection [Chen and Wolf, 1993]. The global coherent dynamics of substorms can be described as the transition between two states (quiet ground state and active state), and this resembles closely a phase transition. The dynamical evolution of substorms in a phase space reconstructed from observational data can be compared with the characteristic temperature–pressure–density (TPD) diagram of equilibrium water–steam system found by Sitnov *et al.* [2000]. On the other hand, the multiscale behavior may be explained by deviations from this low-dimensional picture close to the critical point, characteristic of second-order phase transitions [Stanley, 1971]. Recently, Sitnov *et al.* [2001] have computed a critical exponent of the nonequilibrium transitions in the magnetosphere, which reflects the multiscale aspect of the substorm activity, different from power law frequency and the scale spectra of autonomous systems. This exponent relates input and output parameters of the magnetosphere and is consistent with a second-order phase transition behavior, different from SOC.

[5] The introduction of the concept of nonequilibrium phase transition opens a new area in the study of magnetospheric substorms, as it shows how to reconcile global and multiscale dynamical features in complex systems. The phase transition diagram and multiscale features were obtained by Sitnov *et al.* [2000] from analysis of hundred hours of observed input–output data of the coupled solar wind–magnetosphere system, compiled by Bargatze *et al.* [1985]. The database contains 34 intervals of correlated measurements of the auroral electrojet index AL and solar wind input, each 1–2 days in length. The phase transition-like behavior of the magnetospheric substorms was discovered by reconstructing the dynamical evolution of large number of events.

[6] In the past, the global magnetohydrodynamic (MHD) studies have been focused on the simulation of individual substorm events and comparison with satellite and ground observational data [Fedder *et al.*, 1995; Wiltberger, 1998; Goodrich *et al.*, 1998a, 1998b; Lyon *et al.*, 1998; Lopez *et al.*, 1998; Wiltberger *et al.*, 2000; Papadopoulos *et al.*, 1999; Slinker *et al.*, 2001; Raeder *et al.*, 2001] and were quite successful in reproducing the observed substorm activities in both the magnetosphere and the ionosphere. In this paper, we investigate whether the simulated substorms produced by the global MHD model have the nonequilibrium phase transition-like features as revealed by Sitnov *et al.* [2000]. We simulated seven intervals of total duration of 280 hours from the same Bargatze *et al.* [1985] data set with the LFM global MHD model. Using the same phase space reconstruction techniques as in the studies of Sitnov *et al.* [2000, 2001], we analyzed the input–output system as obtained from the global MHD model and compared the results to those of Sitnov *et al.* [2000, 2001]. It should be emphasized that the main goal of our

study was not to reveal once again the signatures of the phase transition-like behavior of the magnetosphere or elaborate further those ideas (this is being done nowadays in the complementary studies). We considered phase transition signatures first of all as a consistent and convenient set of global and multiscale features of the substorm dynamics, which are useful for statistical verification of various models of the magnetosphere.

[7] In section 2, we introduce the computational model and data processing techniques. In section 3, the pseudo AL index as simulated from the global MHD model is analyzed and compared with the results of Sitnov *et al.* [2000, 2001]. Finally, conclusions are given.

## 2. Input and Output Data

[8] The LFM global MHD model was driven with the solar wind conditions observed by the IMP8 satellite (data available at the data center of UCLA) for seven intervals selected from the Bargatze *et al.* [1985] data set, each 1–2 days in length. The original Bargatze *et al.* [1985] data set contains 34 intervals and is divided into three subsets (1–15, 16–26, and 27–34) representing different levels of substorm activity. Several studies have been conducted with this data set [Blanchard and McPherron, 1993; Smith and Horton, 1998] which contains salient features of substorms. The seven intervals simulated in this paper are chosen from the second Bargatze *et al.* [1985] subset associated with medium activity. The total duration of these seven intervals are around 280 hours. These seven intervals are characterized statistically by simple relation between input and output and are suitable for benchmarking the global MHD simulations statistically. Other intervals with strong activities have not been examined yet and will be examined.

[9] In other words, the driver we used in the global MHD simulation is the solar wind condition observed during the seven intervals which coincide with those in the Bargatze *et al.* [1985] data set. The solar wind variables are the density, velocity (vector), magnetic field (vector), and thermal pressure. The data gaps are filled with interpolated data. These solar wind variables are propagated to the front boundary of the global MHD model in the usual sense described by Wiltberger *et al.* [2000]. The full ionospheric model is used according to the studies of Fedder *et al.* [1995] and Wiltberger *et al.* [2000] and dipole tilt is included.

[10] The simulated magnetospheric and ionospheric response were saved every minute in SM coordinates. With these data files, we built the database of the coupled input–output system given by the global MHD model. The modeled magnetospheric response are sampled at  $x = 20 R_E, y = 0$ , and  $z = 1 R_E$  upstream, which are regarded as the solar wind input. The solar wind input contains several components. Since the substorm activity is closely related to the southward interplanetary magnetic field, in the analysis of this paper, the solar wind input is represented by the induced electric field  $vB_s$ , where  $B_s$  is the southward component of the interplanetary magnetic field (IMF) ( $B_s = 0$  when  $B_z > 0$ ;  $B_s = -B_z$  when  $B_z < 0$ ) and  $v$  is the component of the solar wind velocity along the Earth–Sun axis. The same solar wind input is used by Sitnov *et al.* [2000] and other studies

[Blanchard and McPherron, 1993; Smith and Horton, 1998]. We note that magnetospheric substorms are influenced by many factors other than  $vB_s$ , e.g., solar wind ram pressure and other solar wind magnetic field components, and their physics is still a hotly debated research area. The substorms closely related to the variation of  $vB_s$  belong to a major subclass of the whole family of magnetospheric substorms. Understanding the  $vB_s$ -AL index coupling contributes significantly to the understanding of the magnetospheric substorm physics [Kivelson and Russell, 1995; Vassiliadis et al., 1996; Smith and Horton, 1998].

[11] The pseudo AL index is used as the major measure of the ionospheric response during substorms. The pseudo AL index is produced from the maximum westward ionospheric Hall current that has been searched throughout the grids in the northern hemisphere. Observational AL index is derived from the H component of the magnetic field monitored at 12 stations distributed in longitude. It is obtained from the lower envelope of the single combined plot of the deviations at all stations of the component H magnetic field from its quiet time value [Jursa, 1985]. The observational AL index is a measure of the strength of the auroral electrojet and the AL index perturbations are mainly produced by the E-W (azimuthal) ionospheric Hall current during magnetospheric substorms [Kamide and Baumjohann, 1993]. The pseudo AL index produced from global MHD models is very close to the observed AL index during substorm events. Figure 1 shows examples of the relation between  $vB_s$  and the observed AL index together with the simulated pseudo AL index for two cases from the Bargatze et al. [1985] data set. The top two panels (denoted as Figure 1a) in Figure 1 are for the 16th interval on 27–29 May 1974 in the Bargatze et al. [1985] data set and covers about 35 hours of actual time; the bottom two panels (denoted as Figure 1b) are for the 24th interval on 26–27 August 1974 in the Bargatze et al. [1985] data set and covers about 40 hours. In Figures 1a and 1b, the top panel shows the  $vB_s$  normalized by its standard deviation; the bottom panel shows the observed AL index (solid line) and the simulated pseudo AL index (dotted line), both of which are normalized by their own standard deviation, respectively. Both of the plots in Figure 1 show that the simulated pseudo AL index resembles the observed AL index closely in dynamics. However, it is difficult to judge the closeness directly from the point to point error. Therefore, the coupled  $vB_s$ -pseudo AL index system is analyzed statistically using nonlinear dynamical techniques and compared to the results of Sitnov et al. [2000, 2001] that are based on the analysis of  $vB_s$ -observed AL index system. The idea is to compare the dynamical behavior of the system derived from the MHD simulations to those from the observations.

[12] In the next section, we illustrate the phase space reconstruction technique used to analyze the coupled  $vB_s$ -pseudo AL index data sets.

### 3. Analysis of the Coupled $vB_s$ -Pseudo AL Index System

#### 3.1. Singular Spectrum Analysis (SSA)

[13] A salient feature of a chaotic dynamical system is that the number of variables needed to describe the dynamics can be much smaller than the number of physical

variables [Takens, 1981]. An estimate of the actual number of variables can be obtained from SSA. Following the analysis used by Sitnov et al. [2000], we use a modified SSA or the so-called principal component analysis (PCA) [Broomhead and King, 1986] to include both input and output time series. The input is the product  $vB_s$  time series, essentially the solar wind induced electric field in the  $y$  direction, which is related to the reconnection rate near the Earth's front magnetopause. The output variable is the pseudo AL index produced from the global MHD model. The technique is based on the singular value decomposition (SVD) [Press et al., 1992] of the so-called trajectory matrix constructed from the time series data by time delay embedding:

$$Y(t_i) = (O(t_i), \dots, O(t_i - (m-1)\tau), vB_s(t_i), \dots, vB_s(t_i - (m-1)\tau)), \quad (1)$$

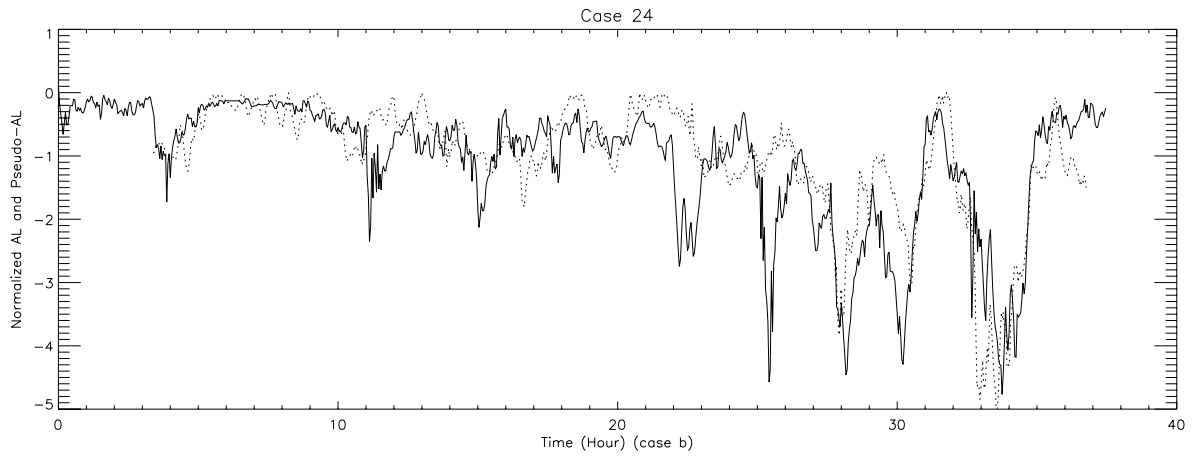
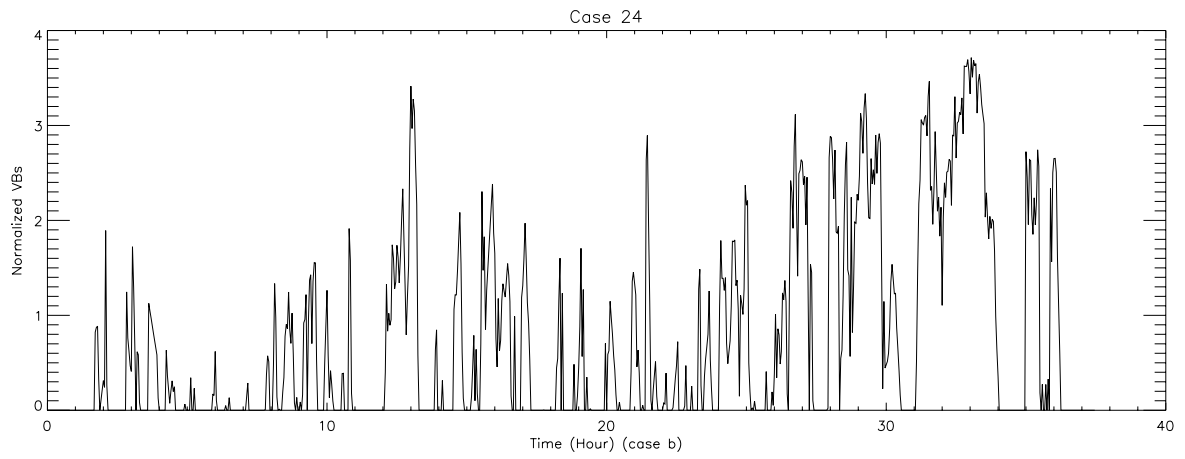
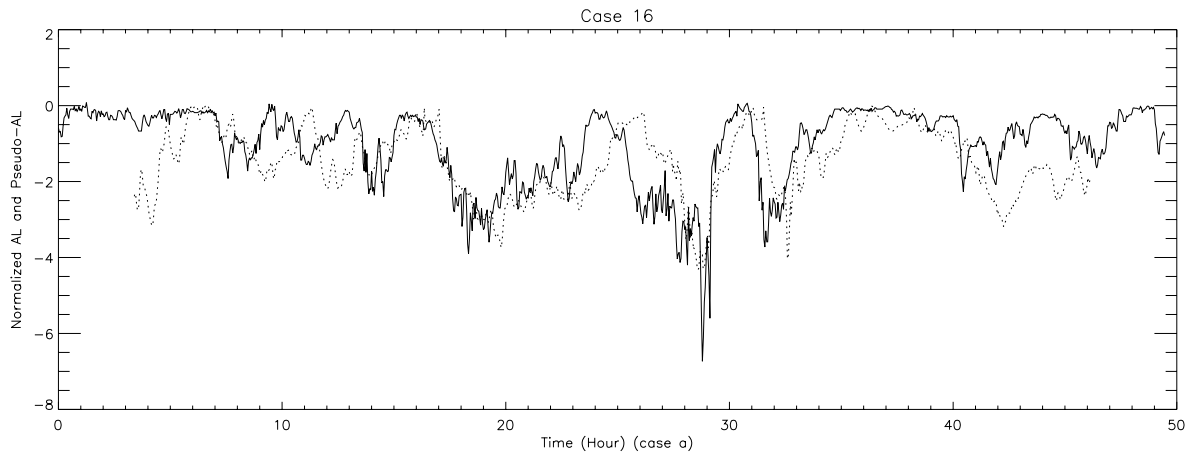
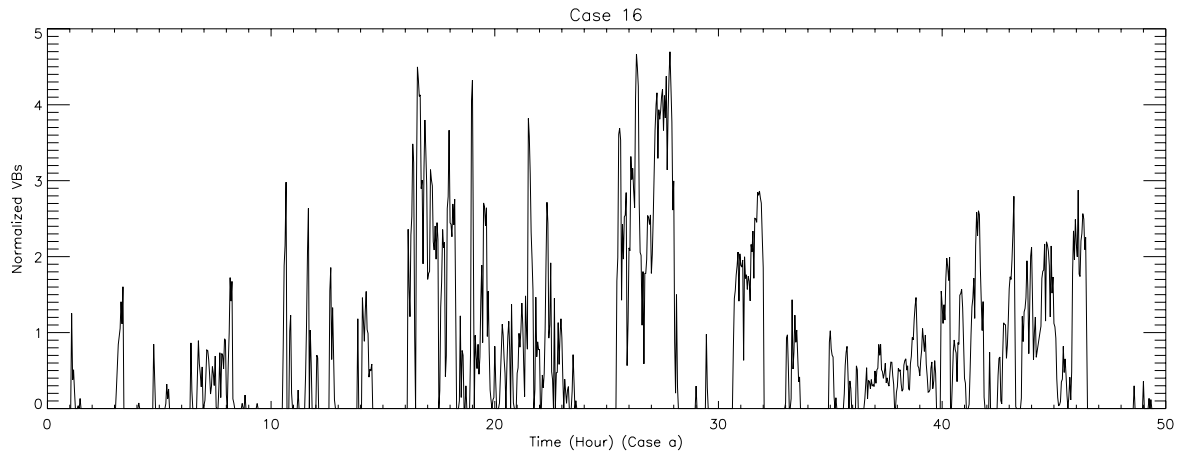
where  $i = 1, \dots, N$ . The time delay  $\tau$  and the embedding dimension  $m$  are chosen from the dynamical properties of the system. The typical value of  $\tau$  is taken to be 2 min and that of the dimension  $m$  of the embedding space is 40, which provide a time window of 80 min comparable to the typical substorm scales. The input and output parameters are normalized separately by the corresponding standard deviations to make them more homogeneous.

[14] This matrix  $\mathbf{Y}$  contains all the dynamical features of the system embodied in the data and the state-space reconstructed by time delay embedding is quite noisy, mainly due to the randomness of the solar wind driver. Since the essential features of the dynamics may be described by a smaller number of linearly independent vectors, the solar wind noise can be removed by the technique of SSA. The matrix  $\mathbf{Y}$  can be represented in the form

$$\mathbf{Y} = \mathbf{U}\mathbf{W}\mathbf{V}^T, \quad (2)$$

using SVD technique. Here,  $\mathbf{U}$  is an  $N \times 2m$  matrix;  $\mathbf{W}$  is a  $2 \times 2m$  diagonal matrix; and  $\mathbf{V}$  is a  $2 \times 2m$  orthogonal matrix. By construction,  $\mathbf{V}^T\mathbf{V}$  is the identity matrix and  $\mathbf{W}$  is a diagonal matrix with the element  $w_j$ , where  $w_j^2$  are the eigenvalues of the semipositive definite matrix  $\mathbf{Y}^T\mathbf{Y}$ .  $\mathbf{V}$  contains the SVD eigenvectors, while  $\mathbf{U}$  determines principal components  $P_j$ , which are the projections of the original trajectory matrix  $\mathbf{Y}$  along the eigenvectors, namely,  $P_j \equiv U_j w_j = (\mathbf{Y}\mathbf{V})_j$ .

[15] For an ideal system, the number of nonzero eigenvalues of  $\mathbf{Y}^T\mathbf{Y}$  gives the number of variables needed to model the system. For a system with noise, SSA can be used to estimate the effective dimension of the system by selecting diagonal element  $w_j$  considerably above a particular noise floor  $w_{fl}$ . Then, the principle components defined by  $P_j$  which corresponds to these  $w_j$  define the corresponding attractor (if it exists) in the embedding space [Ott, 1997]. These linearly independent eigenvectors define the principle directions and thus the principal coordinates in the embedding space, and the time series of these principal variables may be obtained by projecting the given time series onto these directions [Sharma, 1993, 1994; Sharma et al., 1993]. The projected variables may then be used to describe and



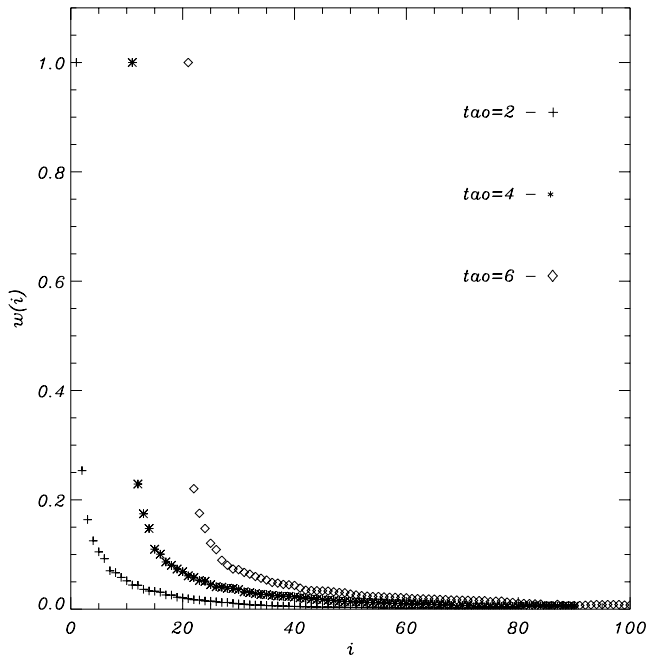


**Figure 2.** Singular spectrum of the coupled  $vB_s$ -pseudo AL index data for different time delay  $\tau = 2.0, 4.0,$  and  $6.0$  min and  $m = 40$ .

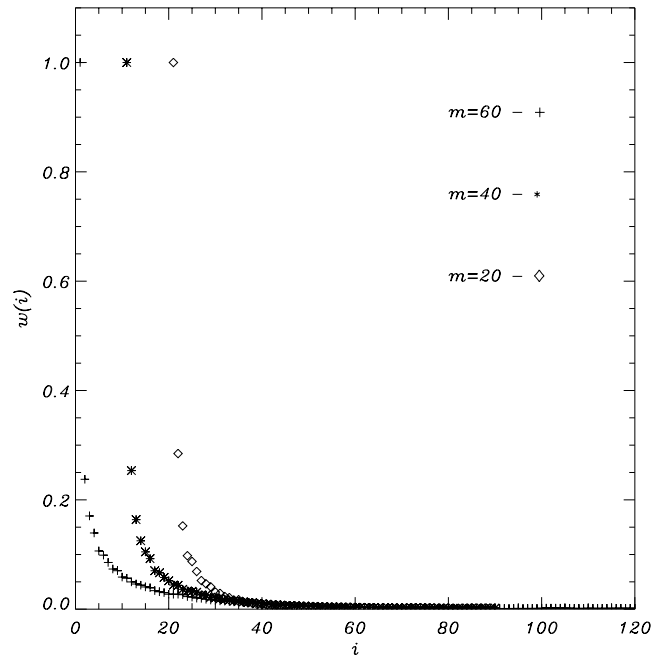


**Figure 3.** Singular spectrum of the coupled  $vB_s$ -pseudo AL index data for different embedding dimension  $m = 20, 40,$  and  $60$  and  $\tau = 2.0$  min.

reconstruct the dynamics. SSA removes the turbulent or random effects and yields the deterministic dynamical features. However, SSA uses linear techniques and consequently the dimension it gives may be considered only as an estimate. SSA may be regarded as a modification of Fourier or wavelet analysis with data-derived basic functions [Preisendorfer, 1988].

### 3.2. Singular Spectrum and Effective Dimension

[16] The singular spectrum of the coupled  $vB_s$ -pseudo AL index data were computed for time delays  $\tau = 2.0, 4.0,$  and  $6.0$  min and for embedding dimensions  $m = 20, 40,$  and  $60$ . These values are chosen to keep the analysis close to the case studied by Sitnov *et al.* [2000], since the time resolution of the two data sets are different. In the study of Sitnov *et al.* [2000],  $\tau = 2.5, 5.0,$  and  $7.5$  min and  $m = 16, 32,$  and  $48$  were used. The total time windows ( $m\tau$ ) are in the range 40–120 min. Figure 2 shows the singular spectrum (eigenvalues  $w_j$ ) for different time delays  $\tau = 2.0, 4.0,$  and  $6.0$  min and embedding dimension  $m = 40$ . Figure 3 shows the eigenvalues for  $\tau = 2.0$  min and different embedding dimension  $m = 20, 40,$  and  $60$ . All the eigenvalues have been normalized to the corresponding maximum eigenvalue.

[17] Figures 2 and 3 show that two or three leading eigenvalues dominate over the others (the fourth eigenvalue is less than 0.15). This is consistent with the results based on the analysis of the coupled  $vB_s$ -observed AL index

system of Sitnov *et al.* [2000]. Here, the second largest eigenvalue is less than 0.3, while in the study of Sitnov *et al.* [2000] the second largest eigenvalue is larger than 0.4. This implies that the leading eigenvectors of the coupled  $vB_s$ -pseudo AL index system which are derived from global MHD model are more dominant. This issue is readdressed in section 3.5 when we discuss the multiscale feature of magnetospheric substorms.

[18] In order to assess the fractal dimension of the system trajectory in the embedding space, we calculate the coastline dimension of the trajectory. The coastline dimension of the trajectory set in the embedding space [Abarbanel *et al.*, 1993] is given by

$$D_f \approx D(N_p) = \log(N_i) / \log(N_p), \quad (3)$$

where  $N_p$  is the number of partitions along each principal component  $P_j$  ( $j = 1, \dots, 4$  as in our case) and  $N_i$  is the number of cubes created because of this partitioning that contain at least one point of the trajectory.

[19] Figure 4 shows the coastline dimension of the coupled  $vB_s$ -pseudo AL index system as a function of the partition  $N_p$  along each of the  $m$  directions in the  $m$ -dimensional embedding space for different  $m = 1, 2, 3,$  and  $4$ . Here, the time delay  $\tau$  is 2 min. Figure 4 shows that when the embedding dimension is increased over 2 ( $m = 3, 4$ ), the coastline dimension converges to  $D_f = 2$ . This is typical of systems with finite dimension. This implies that

**Figure 1.** (opposite) Examples of the relation between  $vB_s$  and the observed and simulated AL index from the Bargatze *et al.* [1985] data set. (a) Top two panels: for the 16th interval on 27–29 May 1974 in the Bargatze *et al.* [1985] data set. (b) Bottom two panels: for the 24th interval on 26–27 August 1974 in the Bargatze *et al.* [1985] data set. In (a) and (b), the top panel shows the  $vB_s$  normalized by its standard deviation. The bottom panel shows the observed AL index (solid line) and the simulated pseudo AL index (dotted line).

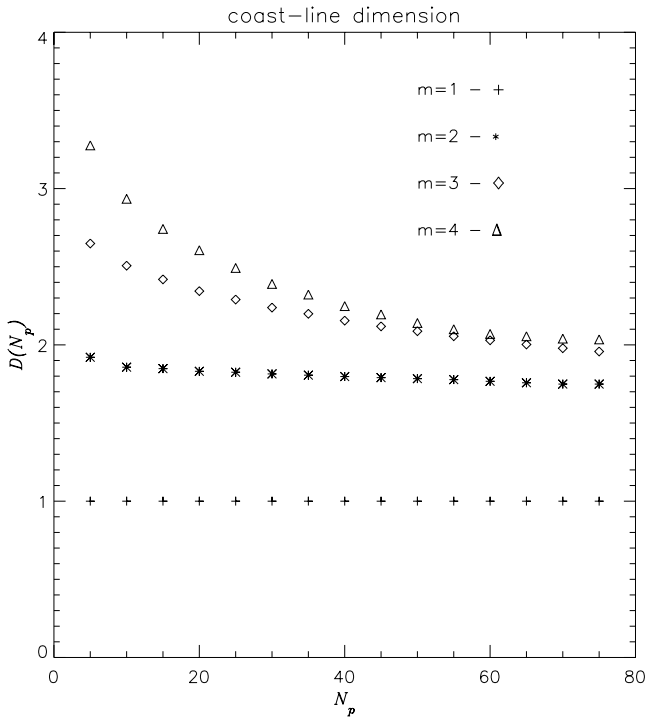


**Figure 4.** Fractal dimension of the coupled  $vB_s$ -pseudo AL index system as a function of the partition  $N_p$ .  $N_p$  is the number of partitions along each of the  $m$  directions in the  $m$ -dimensional embedding space for different  $m = 1, 2, 3$ , and 4.

the trajectory lies mainly on a two-dimensional (2-D) manifold in the embedding space. In the study of *Sitnov et al.* [2000], the coastline dimension of the coupled  $vB_s$ -observed AL index system also converges to  $D_f = 2$  for the embedding dimension larger than 2. Therefore, the coastline dimension of the coupled system derived from the global MHD model is consistent with that of the input-output system based on observations.

[20] Both singular spectrum and fractal dimension analysis show that the manifold on which the trajectory of substorm dynamics lies can be approximated by a 2-D surface. This helps us in reducing effectively the noise and capturing the essential dynamical features of the system obtained from the global MHD simulations. Therefore, we proceed to reconstruct the substorm dynamics in the reduced phase space created by the leading eigenvectors. In the following analysis, the main eigenvectors are limited to be 3. The trajectory matrix  $\mathbf{Y}$  formed with  $\tau = 2$  min and  $m = 40$  is projected onto the three leading eigenvectors. The manifold in the 3-D space is approximated by a 2-D surface.

### 3.3. Original and Rotated Eigenvectors

[21] Figures 5a–5c show the original three leading eigenvectors (the first, second, and third eigenvectors) corresponding to the three largest eigenvalues obtained from the SSA. Each eigenvector is composed of output and input components. The output component  $V(j)$  ( $j = 1-40$ ) is black-shaded and the input component  $V(j)$  ( $j = 41-80$ ) is gray-shaded. As we can see, the input and output components are mixed in each eigenvector.

[22] The ratio between the output and input components are not maximized or minimized in the original eigenvector and make it difficult to visualize and understand the manifold. As suggested by *Sitnov et al.* [2000], we rotate the eigenvector as

$$\begin{cases} V_1 \rightarrow V_1 \cos \alpha + V_2 \sin \alpha \\ V_2 \rightarrow -V_1 \sin \alpha + V_2 \cos \alpha \end{cases} \otimes \begin{cases} V_2 \rightarrow V_2 \cos \beta + V_3 \sin \beta \\ V_3 \rightarrow -V_2 \sin \beta + V_3 \cos \beta \end{cases}. \quad (4)$$

The goal of each rotation is to minimize or maximize the ratio between the output ( $j = 1-40$ ) and input ( $j = 41-80$ ) parts so that the resultant variables approach either the control or state parameter of some catastrophe model. During the first rotation, we maximize the ratio  $|\sum_{j=1}^{40} V_1(j)/\sum_{j=41}^{80} V_1(j)|$ . While for the second rotation, we minimize the ratio  $|\sum_{j=1}^{40} V_2(j)/\sum_{j=41}^{80} V_2(j)|$ . In this way, the first eigenvector is rotated to a direction along which the output component is dominant and the second eigenvector is rotated to a direction along which the input component is dominant. The adjustment is achieved through trial and error and in this case  $\alpha = 0.35$  and  $\beta = 0.30$ . The rotated three leading eigenvectors (we call them basis eigenvectors) are shown in Figures 5d–5f. From Figures 5d–5f, we see that the first vector is dominated by the output part, while the second and the third vector are controlled by the input component. The orthogonality among the three newly obtained basis eigenvectors is maintained.

### 3.4. First-Order Phase Transition-Like Behavior

[23] After obtaining the rotational parameter  $\alpha$  and  $\beta$ , the principle components  $P_j$  ( $j = 1, 2, 3$ ) are projected onto the newly rotated basis vector (shown in Figures 5d–5f). In other words, we are studying the trajectory manifold formed by  $P_j$  ( $j = 1, 2, 3$ ) in the 3-D space with axes formed by the newly obtained basis eigenvectors. Since for the first basis eigenvector, the output component (pseudo AL index) is dominant, we call the corresponding principle component along this eigenvector as  $P_o$ , which is closely related to time-averaged output. For the second basis eigenvector, the input component ( $vB_s$ ) is dominant, and the corresponding principle component is called  $P_i$ .  $P_i$  is closely related to time-averaged input. For the third basis eigenvector, the input component is dominant and experiences one period of oscillation, and the corresponding principle component is called  $P_3$ .  $P_3$  is roughly proportional to the time derivative of the input component.

[24] Figure 6a shows the 2-D surface approximation of the manifold representing magnetospheric dynamics on the basis plane ( $P_3, P_i$ ). The principle component  $P_o$  is color-coded. Surface approximation is achieved through standard triangulation procedure. The circular flows given by  $dP_i/dt$  and  $dP_o/dt$  are represented by arrows. This map is derived from the coupled  $vB_s$ -pseudo AL index system.

[25] Figure 6b, obtained by *Sitnov et al.* [2000], is the similar surface approximation of the manifold to that in Figure 6a. This map is constructed for the coupled  $vB_s$ -observed AL index system derived from the second subset of the *Bargatze et al.* [1985] data set. Figure 6a resembles Figure 6b in the sense that both of the maps capture the phase transition-like behavior qualitatively.

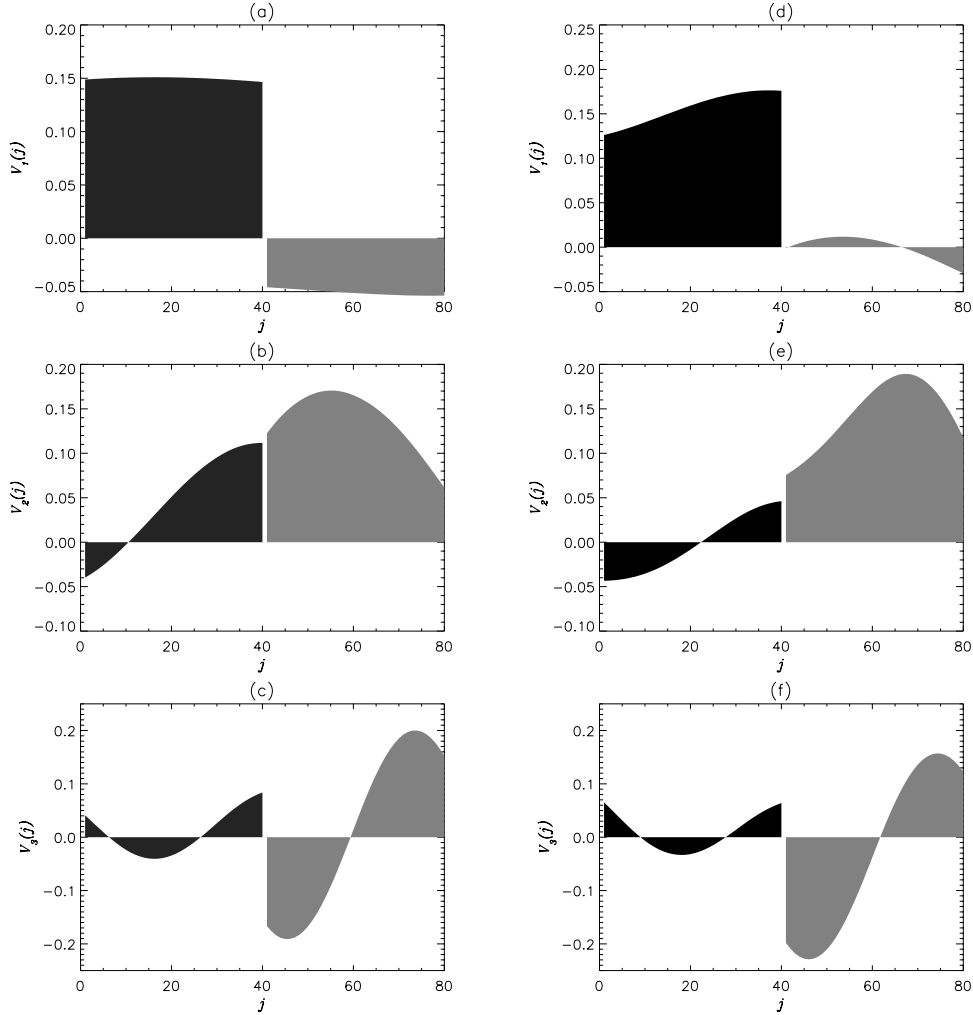


**Figure 5.** (a)–(c) The original three leading eigenvectors obtained from the SSA. (a) The first eigenvector, (b) the second eigenvector, and (c) the third eigenvector. (d)–(f) The three leading eigenvectors after the eigenvectors in (a)–(c) are rotated. (d) Obtained from rotating the eigenvector in (a). (e) Obtained from rotating the eigenvector in (b). (f) Obtained from rotating the eigenvector in (c). Each eigenvector is composed of output and input components. The output component  $V(j)$  ( $j = 1-40$ ) is black-shaded and the input component  $V(j)$  ( $j = 41-80$ ) is gray-shaded.

[26] In Figure 6a,  $P_i = 0$  and  $P_3 = 0$  mark the start of the substorm cycle. The flow arrows show the trajectory of the substorm cycle. During the substorm cycle, when  $P_i$  is increased over zero,  $P_o$  remains nearly 0 and experiences some small decreases (changing from red to yellow). During this interval,  $P_3$  is increased first, then remains nearly constant around 10. This phase corresponds to the growth phase in the substorm cycle. Then  $P_o$  takes large negative values. The flow arrows are the largest during this transition. This rapid transition and the following intensifications (dark blue shaded area) correspond to the expansion phase. The restoration of the system to the original state involves the decrease of  $P_i$  and  $-P_o$ . This phase corresponds to the motion toward left bottom corner and is termed as recovery phase in the substorm cycle.

[27] There have been many discussions regarding the timing of the substorm onset. The coupled input–output system studied here is constructed with the pseudo AL index and  $vB_s$  input. The auroral electrojet index itself alone

is not sufficient to determine the substorm onset, for which combined observations of the auroral image, AL and AE index and tail satellite observations are needed. Furthermore, Figure 6a presents the substorm cycle with  $P_i$  closely related to time-averaged input and  $P_o$  closely related to time-averaged output. Therefore, we do not expect that the transition revealed in Figure 6a by the large falling down will coincide with the usual substorm onset defined from the combination of all available observations. In any case, Figure 6a reconciles the essential features of many substorm cycles revealed by the coupled  $vB_s$ –pseudo AL index on the same map.

[28] Both Figures 6a and 6b are obtained with the same data processing technique, namely SSA. Figure 6a is constructed from the simulated system and Figure 6b is constructed from the real system. Both Figures 6a and 6b show that the evolution of the magnetosphere on the largest scale is quite regular and resembles the temperature–pressure–density diagram of equilibrium phase transition [Stanley,

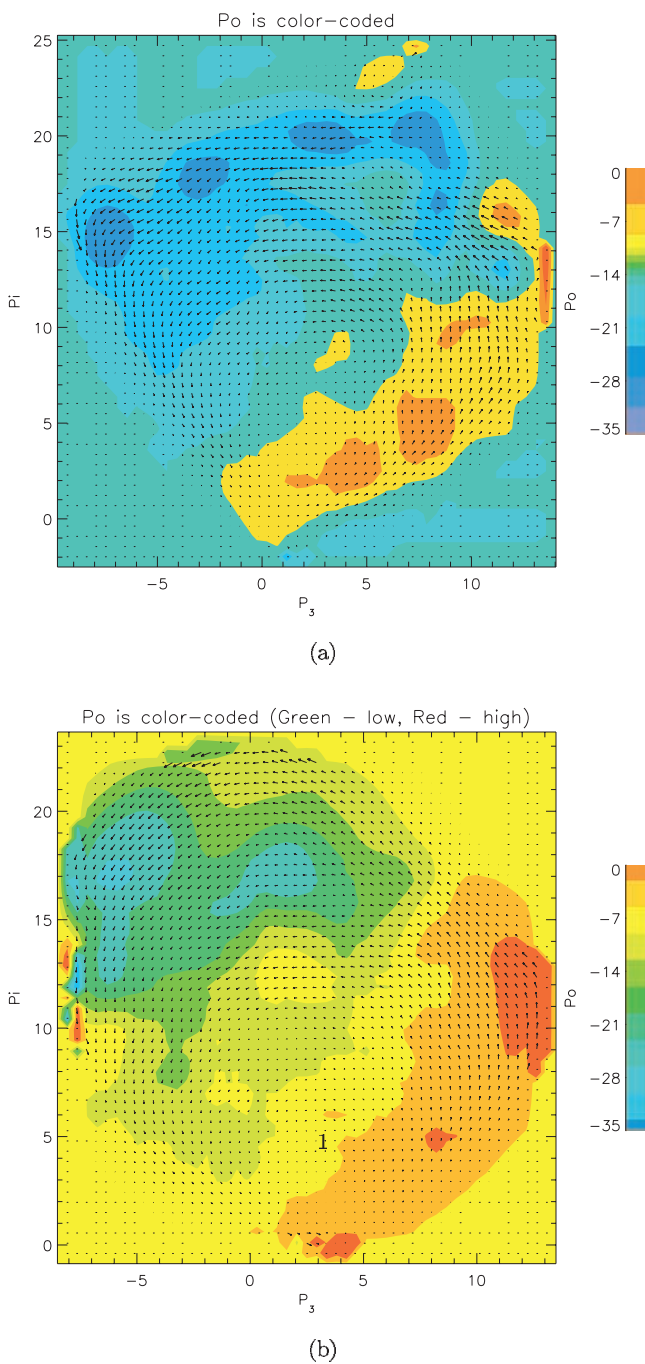


**Figure 6.** (a) The 2-D surface approximation of the manifold representing magnetospheric dynamics on the basis plane ( $P_3$ ,  $P_i$ ). The principle component  $P_o$  is color-coded. The circular flows given by  $dP_i/dt$  and  $dP_o/dt$  are represented by arrows. The phase transition map is obtained from the coupled  $\nu B_s$ -pseudo AL index system. The pseudo AL index is derived from global MHD model. (b) The similar map as in (a) derived by *Sitnov et al.* [2000] for the coupled  $\nu B_s$ -observed AL index system. This map is constructed with the second subset (16–26) of the *Bargatze et al.* [1985] data set.

1971]. The fact that Figure 6a resembles Figure 6b implies that the global MHD model reproduces successfully the phase transition-like behavior that exists in the real substorm cycle. Although, the comparison between observation and individual global MHD simulation may vary, the overall global transition pattern during the substorm cycle revealed by SSA is consistent between simulations and observations. The whole procedure of phase transition analysis using SSA is reliable in the sense that it reveals the qualitative features of global configuration change resides statistically both in the real system and in the global MHD simulation.

[29] As explained by *Sitnov et al.* [2000], both the approximated 2D manifold and the corresponding circulation flows shown in Figure 6a resemble a simple low-dimensional model of a magnetospheric substorm as a cusp catastrophe (inverse bifurcation) [*Gilmore*, 1993]. One of the substorm scenarios based on the cusp catastrophe was proposed by *Lewis* [1991]. Similar low-dimensional models were proposed to explain the substorm activity and used to fit the data by *Baker et al.* [1990], *Klimas et al.* [1992], and *Horton and Doxas* [1996].

[30] Figure 7 shows the schematic cusp catastrophe manifold that was expected to approximate the substorm dynamics of the magnetosphere. The schematic map is similar to the model of *Lewis* [1991]. The evolution of an isolated substorms is shown by dashed arrows.

[31] According to the cusp catastrophe scenario, the dynamics of the magnetosphere is described by the evolution equation for the state parameter  $z$

$$\frac{dz}{dt} = -\frac{\partial U(z, c_1, c_2)}{\partial z}, \quad (5)$$

where the effective potential is defined as

$$U(z, c_1, c_2) = z^4 + 2c_1z^2 + 4c_2z \quad (6)$$

and has two control parameters  $c_1$  and  $c_2$ . These parameters control the quasi-static changes of  $z$ , which is possible as long as the condition  $\frac{\partial U(z, c_1, c_2)}{\partial z} = 0$  is satisfied. The folded surface shown in Figure 7 is determined through this condition.

[32] In the model [*Lewis*, 1991], the state parameter  $z$  is the nightside magnetic field orientation and the control parameters  $c_1 = -(\text{open flux}) + \text{constant}$  and  $c_2 = (\text{nightside} - \text{dayside}) \text{ reconnection rate}$ . In our model, the state parameter is the AL index. The comparison of our results with the general cusp catastrophe model (5) and (6) suggests slightly different interpretation of the control and state parameters. According to panel d in Figure 5, the parameter  $P_i$  resembles the first parameter  $c_1$  of the cusp catastrophe model.  $P_i$  may also be close to the parameter  $c_1$  of *Lewis* [1991] as it is proportional to the inductive electric field  $\nu B_s$  integrated in time. The parameter  $P_3$  is similar to the second parameter  $c_2$  in the model (5) and (6) as it reflects the response of the magnetosphere to solar wind loading. According to panel (f) in Figure 5,  $P_3$  represents the difference between the immediate dayside inductive electric field, which is proportional to  $\nu B_s$  (negative gray bay in Figure 5f) and its delayed value (positive gray bay). The delay is comparable to the propagation time of the signal

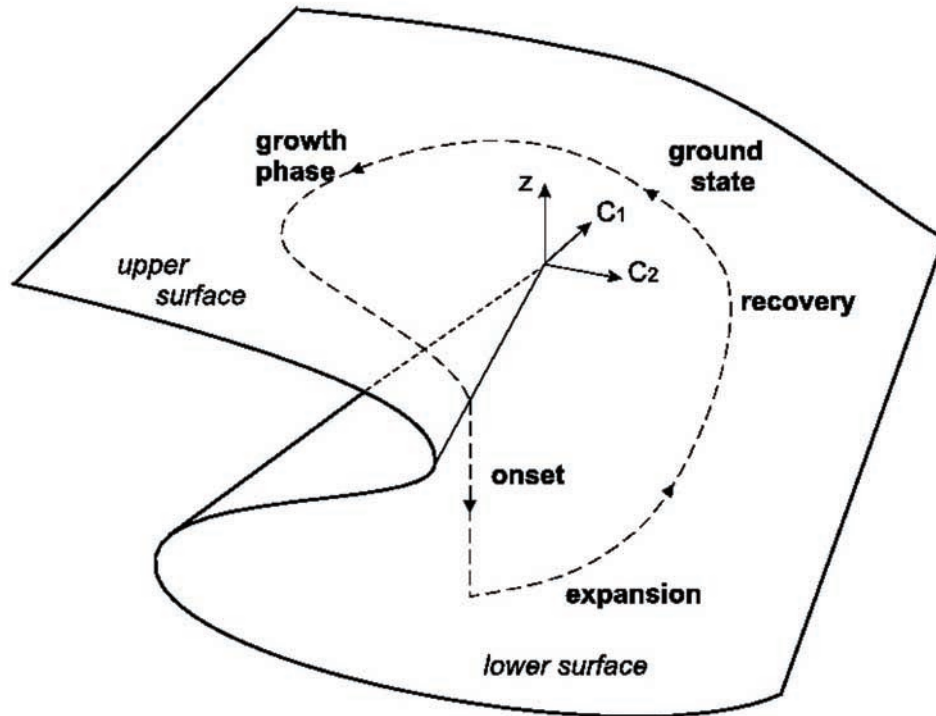


**Figure 7.** Hypothetical cusp catastrophe manifold that was expected to approximate the substorm dynamics of the magnetosphere according to the model of *Lewis* [1991]. The evolution of isolated substorms is shown by dashed arrows.

from the subsolar magnetopause to the distant neutral line. Therefore the delayed component mimics the night side reconnection rate. However, in contrast to the study of *Lewis* [1991], both  $P_i$  and  $P_3$  are characteristics of the solar wind, which controls the magnetospheric activity. This is closer to the original catastrophe scenario (5) and (6) but differs from the interpretation of *Lewis* [1991].

[33] The potential in (6) may have both one and two minima corresponding to different equilibrium states of the system. The onset of the substorm is represented as a local fold catastrophe arising due to the disappearance of the upper potential minimum. In this way, Figure 6a fits into the low-dimensional scheme of magnetospheric substorm as a cusp catastrophe illustrated in Figure 7.

[34] Although catastrophe-like picture can explain the global transition revealed in Figures 6a and 6b on the largest scale, there are still deviations from the ideal catastrophe model. *Sitnov et al.* [2000, 2001] note that the clear first-order phase transition structure gradually disappears with the increase of the average activity. They also observe multiscale features existing with the coupled input–output system. *Sitnov et al.* [2000, 2001] propose another interpretation that accounts for the deviations. The same catastrophe-like picture and multiscale features may be created by dynamical transitions. The bifurcation/catastrophe picture is associated with first-order dynamical phase transitions, while the deviations from the ideal catastrophe picture may be explained by second-order phase transitions near the critical point. The first-order phase transition picture suggests the location of the critical point, which

can be used to obtain the appropriate critical exponent. It is quite interesting to study whether the results from global MHD have multiscale features or not.

### 3.5. Multiscale Behavior

[35] The concept of the SOC is based on a simple model of sandpile [*Bak et al.*, 1987] and has been used widely in the interpretation of catastrophic processes in open spatially extended systems. The SOC concept has been used to explain substorm activity on the basis of the observation that some spectra obey power laws [*Tsurutani et al.*, 1990; *Takalo et al.*, 1993; *Ohtani et al.*, 1995, 1998; *Lui*, 1998; *Uritsky et al.*, 2001]. *Sitnov et al.* [2000] suggest that scale-invariant or multiscale behavior originates from the second-order phase transitions instead of SOC.

[36] SOC models emphasize that the input is not essential because of the self-tuning properties of the system and provide only one class of critical exponents, which relate some parameter of the system, such as the energy released with the spatial scale or characteristic frequency. While the second-order phase transitions have at least one more class of critical exponents that relate the input parameter of the system, e.g., magnetic field or temperature, with its output, e.g., magnetization or density. *Vespignani and Zapperi* [1998] showed that the SOC state requires tuning and consequently there are several scaling relationship between input, output, and the internal state of the system. *Chang et al.* [2001] point out that the paradigm “Forced SOC” (FSOC) is more appropriate to describe the criticality behavior involved with input or controlling parameters. We feel that this falls

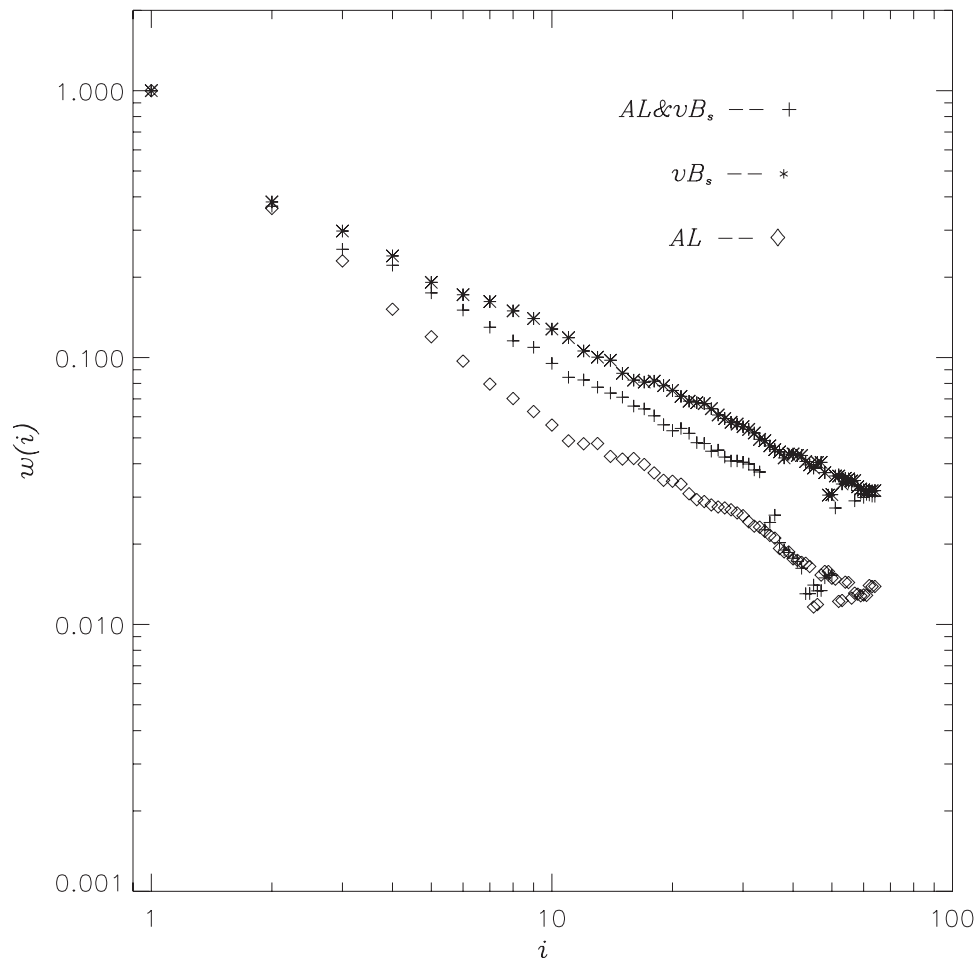


**Figure 8.** Log-log plots of SSA eigenvalues for observed AL or pseudo AL index and  $vB_s$  parameters alone as well as for the combined data in cases of the coupled  $vB_s$ -observed AL index system from the study of *Sitnov et al.* [2000].  $\tau = 2.5$  min,  $m = 32$  in the case of combined data and  $m = 64$  for input and output parameters alone.

into the category of second-order phase transition and is not SOC any more. In the studies of *Sitnov et al.* [2000, 2001], two kinds of critical exponents are found with the new data-derived image of substorms. The first critical exponent is related to the scale-invariant (or power law) behavior of the eigenvalues obtained from SSA as shown in Figure 8. Figure 8 shows the singular spectra of the coupled  $vB_s$ -observed AL index system of *Sitnov et al.* [2000] on log-log plot. The second critical exponent, which is the primary distinctive feature between second-order phase transition and SOC, is derived from the envelope  $\max(-dP_o/dt)$  of the velocity time series  $v(t_i) = dP_o/dt$ . In other words, given  $P_i$ , which is closely related to the time-averaged input, there is a maximum decreasing rate for  $P_o$  and  $\max(-dP_o/dt)$  scales in power law with  $P_i$ . Using an analogy to the dynamical Ising model in the mean field approximation, the connection between the data-derived exponent of nonequilibrium transitions in the magnetosphere and the standard critical exponent  $\beta$  of equilibrium second-order phase transitions is shown to be  $\beta = \beta_w/3$ . *Sitnov et al.* [2000, 2001] conclude that the substorm dynamics of the magnetosphere resembles more the conventional set of first and second-order phase transitions rather than SOC or catastrophe model. In this section, we investigate these two kinds of critical exponents using the

global MHD simulations and compare them to the results of *Sitnov et al.* [2000, 2001].

[37] Figure 9 shows the singular spectra of the coupled  $vB_s$ -pseudo AL index system derived from the global MHD model on log-log plot. Figure 8 indicates that the singular spectrum of the observed AL index data alone obeys power law with an exponent around  $-1$ . Figure 9 indicates that the singular spectrum of the pseudo AL index data alone also obeys power law with an exponent around  $-1.5$ . Both the observed AL index and the pseudo AL index show multiscale behavior. But, the pseudo AL index is much cleaner than the observed AL index in the sense that its singular spectrum assumes steeper slope (in log-log plot). This is because the global MHD model works on large scales and low frequency regions and smoothes local and high frequency fluctuations. Figure 8 also shows that the singular spectrum of the combined  $vB_s$  and observed AL index data obeys power law and assumes the slope (in log-log plot) in between those of the singular spectra of the  $vB_s$  data and the observed AL index data, separately. In Figure 8, the singular spectrum of the combined  $vB_s$  and pseudo AL index data spreads for  $i > 40$ . While for the singular spectrum of the combined  $vB_s$  and pseudo AL index data (in Figure 9), the slope of the singular spectrum changes

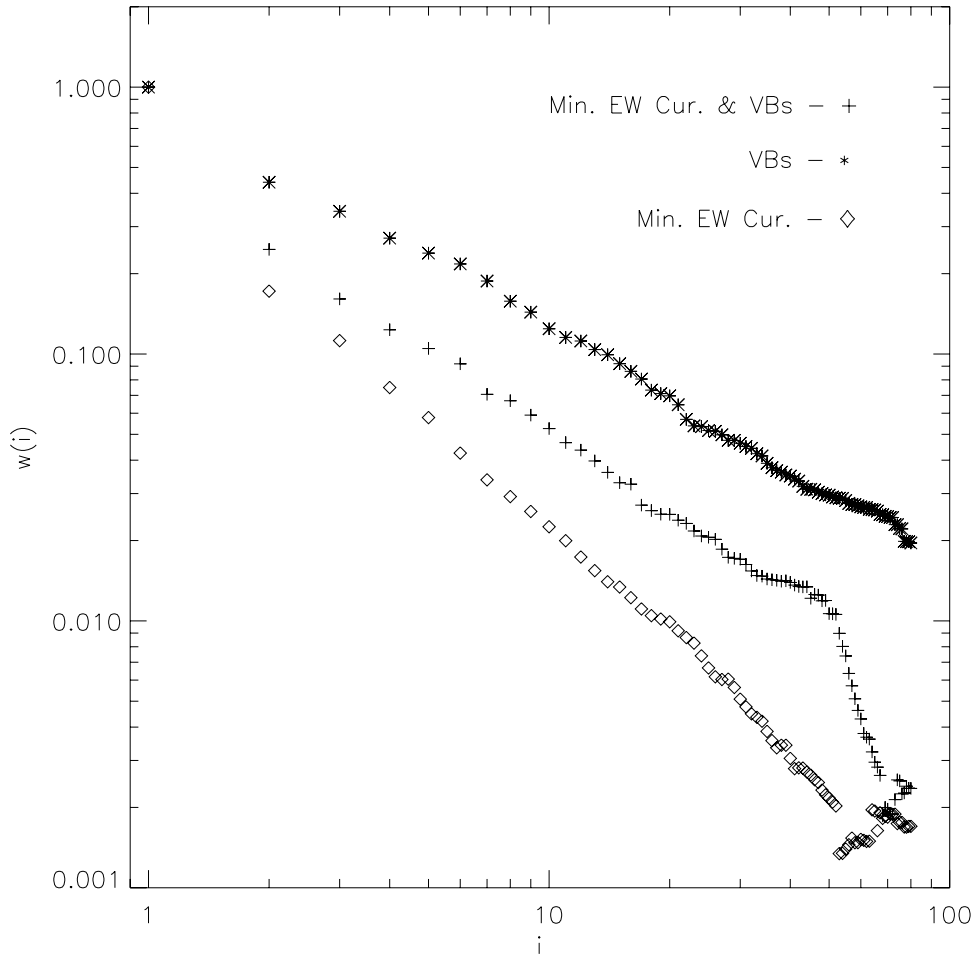


**Figure 9.** Log-log plots of SSA eigenvalues for observed AL or pseudo AL index and  $\nu B_s$  parameters alone as well as for the combined data in cases of the coupled  $\nu B_s$ –pseudo AL index system derived from global MHD model.  $\tau = 2$  min,  $m = 40$  in the case of combined data and  $m = 80$  for input and output parameters alone.

around  $i = 50$ . In Figure 9, the slope of the spectrum of the combined data is  $-1.33$  for  $i < 50$  and changes to  $-3$  for  $i > 50$ . For higher SSA components of the combined data derived from the global MHD model, the spectrum decays faster and the corresponding principle component is less important.

[38] Figure 10 shows the rate of the positive and negative changes of the parameter  $P_o$  as a function of  $P_i$  obtained from the analysis of the global MHD model data. The bottom left and right curves marks the lower envelope of the changing rate of  $P_o$ . We can clearly see that there are two envelopes. For the positive values of  $dP_o/dt$ , which corresponds to the recovery phase of substorms, the envelope is a straight line. While for the negative values of  $dP_o/dt$ , which corresponds to the active period (decrease of pseudo AL index), the envelope is a curve. With the increase of  $P_i$ , the maximum of  $(-dP_o/dt)$  increases.

[39] Figure 11 shows the similar plot of  $dP_o/dt$  versus  $P_i$  obtained from the coupled  $\nu B_s$ –observed AL index system studied by *Sitnov et al.* [2001]. We can see that Figure 10 resembles Figure 11 in the sense that both of the plots show similar envelopes. The curved envelopes in Figures 10 and 11

are of interest, since they are related closely to the input and output parameter.

[40] Figures 12 and 13 show the log-log plots of the lower (curved) envelopes in Figures 10 and 11, respectively. In Figure 12, the two lines are of slopes 0.7 and 0.4, separately. They correspond to the two curve in Figure 10, respectively. While in Figure 13, the dash line is of slope 0.64. We can see that the curved envelope derived from the coupled  $\nu B_s$ –observed AL index system (in Figure 11) obeys a power law that spans four decades. The curved envelope derived from the coupled  $\nu B_s$ –pseudo AL index system (in Figure 10) shows two slopes. When the parameter  $P_i$  is small ( $< 1.0$ ), the curved envelope in Figure 10 scales with a power close to that of the real system. When the parameter  $P_i$  is large ( $> 1.0$ ), the curved envelope in Figure 10 scales with another power smaller than that of the real system. With the increase of the input  $\nu B_s$ , the maximum changing rate of  $(-P_o)$  does not increase as fast as in the case derived from observations. Our explanation is that in the global MHD model, which has only an electrostatic model of the ionosphere and does not have a ring current in the magnetosphere, the ionospheric activity can be underestimated with excessive input.

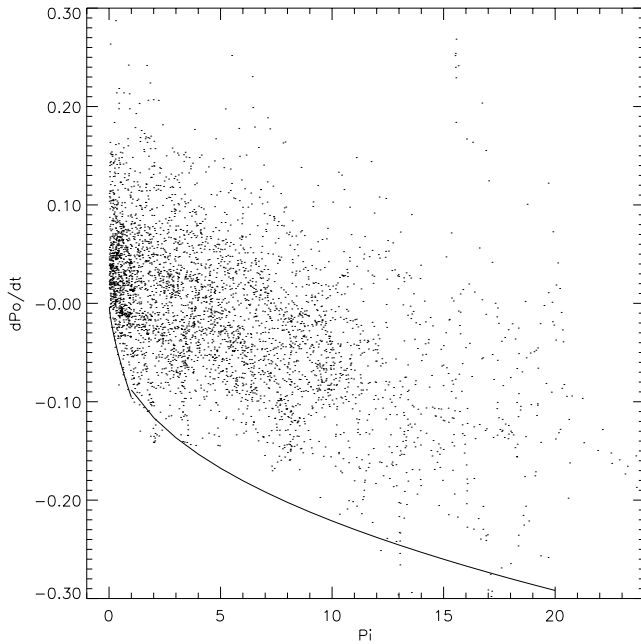


**Figure 10.** Rate of the positive and negative changes of the parameter  $P_o$  as a function of  $P_i$  obtained from the analysis of the global MHD model data. The bottom left and right curves mark the lower envelope of the changing rate of  $P_o$  as a function of  $P_i$ .

[41] The global MHD simulation data reveal the curved envelope relation between  $P_i$  and  $\max(-dP_o/dt)$ , as in the real system.  $P_i$  and  $P_o$  are closely related to input and output parameter. The envelope of  $\max(-dP_o/dt)$  scales as  $P_i$  with two envelopes. Therefore, to some degree, the global MHD model reveals the multiscale behavior. Both the analysis of the real system and that of the global MHD model show that

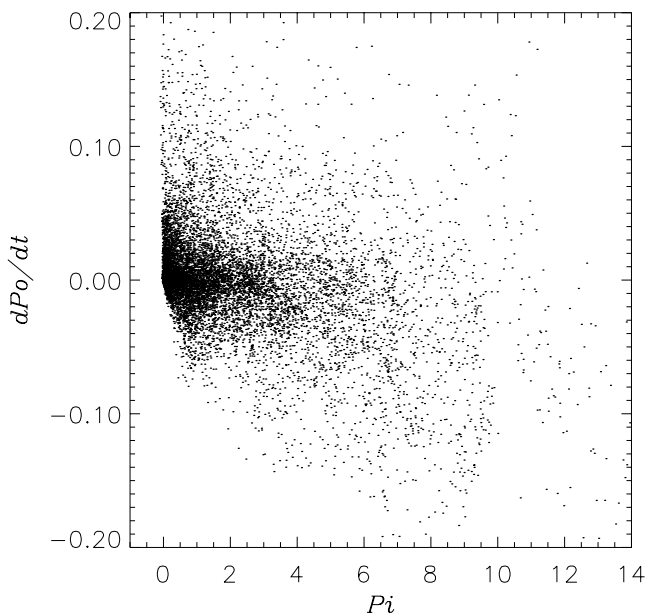


**Figure 11.** Rate of the positive and negative changes of the parameter  $P_o$  as a function of  $P_i$  obtained from the coupled  $\nu B_s$ -observed AL index system studied by *Sitnov et al.* [2001].

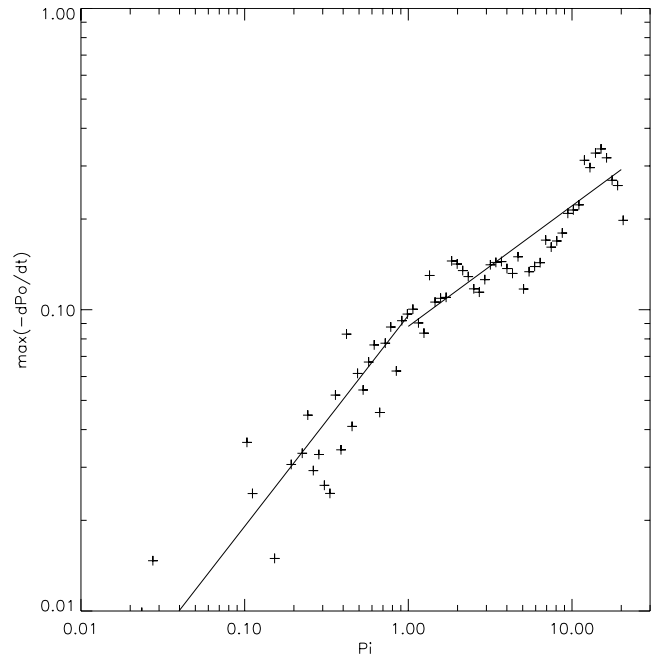


**Figure 12.** Log-log plot of the lower envelope in Figure 10.

the magnetosphere resembles the conventional set of first and second-order phase transition rather than SOC or catastrophe model.

#### 4. Conclusions

[42] In this paper, we use techniques of SSA to analyze the coupled input-output system derived from the global MHD simulations and compare the results to those from the analysis of the observations by *Sitnov et al.* [2000, 2001]. The conclusions are listed as following:

1. The analysis of the coupled  $\nu B_s$ -pseudo AL index system derived from the global MHD simulations shows the first-order phase transition map, which is consistent with the

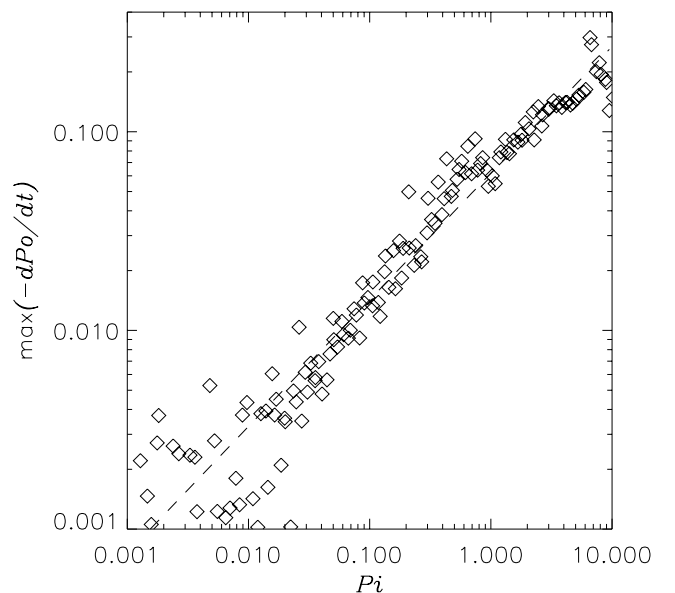


**Figure 13.** Log-log plot of the lower envelope in Figure 11.

similar map obtained for the  $vB_s$ -observed AL index system of *Sitnov et al.* [2000, 2001]. The reconstructed surface resembles the so-called temperature–pressure–density diagram for the equilibrium first-order phase transitions [e.g., *Stanley*, 1971]. Although, the comparison between observation and individual global MHD simulation may vary, the overall global transition pattern during the substorm cycle revealed by SSA is consistent between simulations and observations. The procedure of phase transition analysis using SSA has revealed the qualitative features of global configuration change both in the real system and in the global MHD simulations.

2. The bifurcation/catastrophe picture is associated with first-order dynamical phase transitions, while the deviations from the ideal catastrophe picture may be explained by second-order phase transitions near the critical point. The coupled  $vB_s$ -pseudo AL index system derived from global MHD simulations shows multiscale behavior (scale-invariant power law dependence) in singular power spectrum. The pseudo AL index is much cleaner than the observed AL index in the sense that its singular spectrum assumes more steep slope (in log-log plot).

[43] The global MHD simulation data reveal the curved envelope relation between  $P_i$  and  $\max(-dP_o/dt)$ , as in the real system.  $P_i$  and  $P_o$  are closely related to the input and output parameter, respectively. The envelope of  $\max(-dP_o/dt)$  scales as  $P_i$  with two exponents. With the increase of the input  $vB_s$ , the maximum changing rate of  $(-P_o)$  does not increase as fast as in the case derived from observations. Our explanation is that in the global MHD model, which has only an electrostatic model of the ionosphere and does not have ring current in the magnetosphere, the ionospheric activity can be underestimated with excessive input. In any case, the curved envelope relation between  $P_i$  and  $\max(-dP_o/dt)$  is the essential feature which distinguish the second-order phase transition model from the SOC model.

[44] We point out that the intervals used in this paper are associated with medium activity substorms and are suitable for benchmarking the global MHD simulations statistically. Other intervals with strong activities have not been examined yet and will be examined.

[45] In summary, the global MHD simulation results are shown to statistically reproduce both global coherent and multiscale features of the substorm dynamics of the Earth's magnetosphere. Global MHD simulations are thus proven to be an efficient instrument in modeling magnetosphere. On the other hand, they can be used as a test bed of more general studies of complexity in open systems.

[46] **Acknowledgments.** CDAweb and UCLA Institute of Geophysics and Planetary Physics (IGPP) Space Physics Center provided the IMP-8 data. Scientific computations were performed on Cray J90 and Cray SV1 supercomputers at the Texas Advanced Computing Center (TACC) and on ORIGIN2000 at the National Computational Science Alliance (NCSA), University of Illinois at Urbana-Champaign. This work was supported in part by the ISTP program NAG-51101 sponsored by NASA, NSF grants ATM-0003188 and ATM-0001676, and NCSA grant MCA01S003N. X. Shao thanks the National Research Council and NSSDC for providing him a postdoc position in NSSDC, NASA.

## References

Arbanel, H. D., R. Brown, J. J. Sidorovich, and T. S. Tsimring, The analysis of observed chaotic data in physical systems, *Rev. Mod. Phys.*, **65**, 1331, 1993.

- Bak, P., C. Tang, and K. Wiesenfeld, Self-organized criticality: An explanation of  $1/f$  noise, *Phys. Rev. Lett.*, **50**, 381–384, 1987.
- Baker, D. N., A. J. Klimas, R. L. McPherron, and J. Büchner, The evolution from weak to strong geomagnetic activity: An interpretation in terms of deterministic chaos, *Geophys. Res. Lett.*, **17**, 41, 1990.
- Baker, D. N., T. Pulkkinen, V. Angelopoulos, W. Baumjohann, and R. L. McPherron, Neutral line model of substorm: Past results and present view, *J. Geophys. Res.*, **101**, 12,975, 1996.
- Bargatze, L. F., et al., Magnetospheric impulse response for many levels of geomagnetic activity, *J. Geophys. Res.*, **90**, 6387, 1985.
- Blanchard, G. T., and R. L. McPherron, A bimodal representation of the response function relating the solar wind electric field to the AL index, *Adv. Space Res.*, **13**(4), 71, 1993.
- Broomhead, D. S., and G. P. King, Extracting qualitative dynamics from experimental data, *Physica D*, **20**, 217, 1986.
- Chang, T., S. Chapman, and A. Klimas, Forced and/or self-organized criticality (FSOC) in space plasmas: Preface, *J. Atmos. Sol. Terr. Phys.*, **63**, 1359, 2001.
- Chapman, S. C., N. W. Watkins, R. O. Dendy, and G. Rowlands, A simple avalanche model as an analogue for magnetospheric activity, *Geophys. Res. Lett.*, **25**, 2397, 1998.
- Chen, C. X., and R. A. Wolf, Interpretation of high-speed flows in the plasma sheet, *J. Geophys. Res.*, **98**, 21,409, 1993.
- Consolini, G., Sandpile cellular automata and magnetospheric dynamics, in *Proceedings of the 8th GIFCO Conference, Cosmic Physics in the Year 2000: Scientific Perspectives and New Instrumentations, 8–10 April 1997*, edited by S. Aiello et al., pp. 123–126, Soc. Ital. di Fis., Bologna, Italy, 1997.
- Fedder, J. A., S. P. Slinker, J. G. Lyon, and R. D. Elphinstone, Global numerical simulation of the growth phase and the expansion onset for substorm observed by Viking, *J. Geophys. Res.*, **100**, 19,083, 1995.
- Gilmore, R., *Catastrophe Theory for Scientists and Engineers*, Dover, Mineola, N. Y., 1993.
- Goodrich, C. C., M. Wiltberger, R. E. Lopez, K. Papadopoulos, and J. G. Lyon, An overview of the impact of the January 10–11, 1997 magnetic cloud on the magnetosphere via global MHD simulation, *Geophys. Res. Lett.*, **25**, 2537–2540, 1998a.
- Goodrich, C. C., M. Wiltberger, R. E. Lopez, K. Papadopoulos, and J. G. Lyon, Global MHD simulations of actual magnetospheric substorm events, in *Substorms-4*, edited by S. Kokubun and Y. Kamide, pp. 645–649, Terra Sci., Tokyo, 1998b.
- Horton, W., and I. Doxas, A low dimensional energy conserving state space model for substorm dynamics, *J. Geophys. Res.*, **101**, 27,223, 1996.
- Jursa, A. S., *Handbook of Geophysics and the Space Environment*, Air Force Geophys. Lab., Hanscom Air Force Base, Mass., 1985.
- Kamide, Y., and W. Baumjohann, *Physics and Chemistry in Space*, vol. 23, *Mesosphere–Ionosphere Coupling*, Springer-Verlag, New York, 1993.
- Kivelson, M. G., and C. T. Russell, *Introduction to Space Physics*, Cambridge Univ. Press, New York, 1995.
- Klimas, A. J., D. N. Baker, D. A. Roberts, D. H. Fairfield, and J. Büchner, A nonlinear dynamical analogue model of geomagnetic activity, *J. Geophys. Res.*, **97**, 12,253, 1992.
- Klimas, A. J., D. Vassiliadis, D. N. Baker, and D. A. Roberts, The organized nonlinear dynamics of the magnetosphere, *J. Geophys. Res.*, **101**, 13,089, 1996.
- Klimas, A. J., J. A. Valdivia, D. Vassiliadis, D. N. Baker, M. Hesse, and J. Takalo, Self-organized criticality in the substorm phenomenon and its relation to localized reconnection in the magnetospheric plasma sheet, *J. Geophys. Res.*, **105**, 18,765, 2000.
- Lewis, Z. V., On the apparent randomness of substorm onset, *Geophys. Res. Lett.*, **18**, 1627, 1991.
- Lopez, R. E., C. C. Goodrich, M. Wiltberger, and J. G. Lyon, Simulation of the March 9, 1995 substorm and initial comparison to data, in *Geospace Mass and Energy Flow: Results from the International Solar-Terrestrial Physics Program*, *Geophys. Monogr.*, vol. 104, edited by J. L. Horowitz, D. L. Gallagher, and W. K. Peterson, 237–245, AGU, 1998.
- Lui, A. T. Y., Multiscale and intermittent nature of current disruption in the magnetotail, in *Physics of Space Plasmas*, vol. 15, edited by T. Chang and J. R. Jasperse, p. 233, Mass. Inst. Technol. Cent. for Geo/Cosmo Plasma Phys., Cambridge, 1998.
- Lui, A. T. Y., et al., Is the dynamic magnetosphere an avalanching system?, *Geophys. Res. Lett.*, **27**, 911, 2000.
- Lyon, J. G., R. E. Lopez, C. Goodrich, M. Wiltberger, and K. Papadopoulos, Simulation of the March 9, 1995, substorm: Auroral brightening and the onset of lobe reconnection, *Geophys. Res. Lett.*, **25**, 3039–3042, 1998.
- Ohtani, S., T. Higuchi, A. T. Y. Lui, and K. Takahashi, Magnetic fluctuations associated with tail current disruption: Fractal analysis, *J. Geophys. Res.*, **100**, 19,135, 1995.

- Ohtani, S., T. Higuchi, A. T. Y. Lui, and K. Takahashi, AMPTE/CCE-SCATHA simultaneous observations of substorm-associated magnetic fluctuations, *J. Geophys. Res.*, *103*, 4671–4682, 1998.
- Ott, E., *Chaos in Dynamical Systems*, Cambridge Univ. Press, New York, 1997.
- Papadopoulos, K., C. Goodrich, M. Wiltberger, R. Lopez, and J. G. Lyon, The Physics of Substorms as revealed by ISTP, *Phys. Chem. Earth, Part C*, *24*(1–3), 189–202, 1999.
- Preisendorfer, R. W., *Principal Component Analysis in Meteorology and Oceanography*, 425 pp., Elsevier Sci., New York, 1988.
- Press, W. H., B. P. Flannery, S. A. Teukolsky, and W. V. Vetterling, *Numerical Recipes: The Art of Scientific Computing*, 2nd ed., Cambridge Univ. Press, New York, 1992.
- Raeder, J., R. L. McPherron, L. A. Frank, S. Kokubun, G. Lu, T. Mukai, W. R. Paterson, J. B. Sigwarth, H. J. Singer, and J. A. Slavin, Global simulation of the Geospace Environment Modeling substorm challenge event, *J. Geophys. Res.*, *106*, 381, 2001.
- Sergeev, V. A., T. I. Pulkkinen, and R. J. Pellinen, Coupled mode scenario for the magnetospheric dynamics, *J. Geophys. Res.*, *101*, 13,047, 1996.
- Sharma, A. S., Nonlinear dynamics of space plasmas and predictive modeling, in *Recent Trends in Nonlinear Space Plasmas*, edited by R. Z. Sagdeev, p. 141, Am. Inst. Phys., New York, 1993.
- Sharma, A. S., Reconstruction of phase space from time series data by singular spectrum analysis, in *Physics of Space Plasmas*, vol. 13, edited by T. Chang and J. R. Jasperse, p. 423, Mass. Inst. Technol. Cent. for Theor. Geo/Cosmo Plasma Phys., Cambridge, 1994.
- Sharma, A. S., Assessing the magnetosphere's nonlinear behavior: Its dimension is low, its predictability is high, *Rev. Geophys.*, *33*, 645, suppl., 1995.
- Sharma, A. S., D. Vassiliadis, and K. Papadopoulos, Reconstruction of low-dimensional magnetospheric dynamics by singular spectrum analysis, *Geophys. Res. Lett.*, *20*, 335, 1993.
- Sitnov, M. I., A. S. Sharma, K. Papadopoulos, D. Vassiliadis, J. A. Valdivia, A. J. Klimas, and D. N. Baker, Phase transition-like behavior of the magnetosphere during substorms, *J. Geophys. Res.*, *105*, 12,955, 2000.
- Sitnov, M. I., A. S. Sharma, K. Papadopoulos, and D. Vassiliadis, Modeling substorm dynamics of the magnetosphere: From self-organization and self-organized criticality to nonequilibrium phase transitions, *Phys. Rev.*, *65*, 16,116, 2001.
- Slinker, S. P., J. A. Fedder, J. M. Ruohoniemi, and J. G. Lyon, Global MHD simulation of the magnetosphere for November 24, 1996, *J. Geophys. Res.*, *106*, 361, 2001.
- Smith, J. P., and W. Horton, Analysis of the bimodal nature of solar wind–magnetosphere coupling, *J. Geophys. Res.*, *103*, 14,917, 1998.
- Stanley, H. E., *Introduction to Phase Transition and Critical Phenomena*, Oxford Univ. Press, New York, 1971.
- Takalo, J., J. Timonen, and H. Koskinen, Correlation dimension and affinity of AE data and bicolored noise, *Geophys. Res. Lett.*, *20*, 1527, 1993.
- Takens, F., Detecting strange attractors in turbulence, in *Dynamical Systems and Turbulence*, pp. 366–381, Springer-Verlag, New York, 1981.
- Tsurutani, B., M. Sugiura, T. Iyemori, B. E. Goldstein, W. D. Gonzalez, and E. J. Smith, The nonlinear response of AE to the IMF Bs, *Geophys. Res. Lett.*, *17*, 279, 1990.
- Uritsky, V. M., A. J. Klimas, and D. Vassiliadis, Comparative study of dynamical critical scaling in the auroral electrojet index versus solar wind fluctuations, *Geophys. Res. Lett.*, *28*, 3809, 2001.
- Vassiliadis, D., A. J. Klimas, D. N. Baker, and D. A. Roberts, The non-linearity of models of the  $vB_{South-AL}$  coupling, *J. Geophys. Res.*, *101*, 19,779, 1996.
- Vespignani, A., and S. Zapperi, How self-organized criticality works: A unified mean-field picture, *Phys. Rev. E*, *57*, 6345, 1998.
- Wiltberger, M., Global magnetohydrodynamic simulations of magnetospheric substorms, Ph.D. dissertation, Univ. of Maryland, College Park, 1998.
- Wiltberger, M., T. I. Pulkkinen, J. G. Lyon, and C. C. Goodrich, MHD simulation of the magnetotail during the December 10, 1996, substorm, *J. Geophys. Res.*, *105*, 27,649, 2000.

---

C. C. Goodrich, G. M. Milikh, K. Papadopoulos, X. Shao, S. A. Sharma, and M. I. Sitnov, Department of Astronomy, University of Maryland, College Park, MD 20742, USA. (ccg@avl.umd.edu; milikh@astro.umd.edu; kp@astro.umd.edu; xshcn@astro.umd.edu; ssh@astro.umd.edu; sitnov@astro.umd.edu)

P. N. Guzdar, Institute for Plasma Research, University of Maryland, College Park, MD 20742, USA. (guzdar@ipr.umd.edu)

J. G. Lyon and M. J. Wiltberger, Department of Astronomy, Dartmouth College, Hanover, NH 03755, USA. (lyon@tinman.dartmouth.edu; wiltbemj@tinman.dartmouth.edu)